Digest Journal of Nanomaterials and Biostructures Vol. 12, No. 4, October-December 2017, p. 1031-1039

EFFECT OF SINTERING TEMPERATURE ON NANOSTRUCTURE AND GRAIN BOUNDARY DIFFUSION OF PLASMA SPRAYABLE CALCINED NiO-8YSZ CERMET PARTICLES

J. K. JEONG[a†], I. H. HWANG[b†], K. T. LIM[c], J. M. JUNG[a,d*]
[a]*Division of Mechanical Design Engineering, Chonbuk National University, Jeonju 54596, South Korea*
[b]*Department of Bio-Nano System Engineering, Chonbuk National University, Jeonju 54596, South Korea*
[c]*Kceracell, Geumsan 32702, South Korea*
[d]*Hemorheology Research Institute, Chonbuk National University, Jeonju 54596, South Korea*

The plasma spray technique was employed to produce an anode layer for solid oxide fuel cells (SOFCs) using calcined micro-sized nickel oxide-8 mol% yttria-stabilized zirconia (NiO-8YSZ) cermet particles as stock powder. The nanostructure of calcined micro-sized NiO-8YSZ cermet particles (CMCEP) generated through the sintering process is closely related to SOFC performance and varied with sintering conditions. Thus, the present study was conducted to analyze the effect of the sintering temperature on the diffusion and nanostructure of particles during the production of CMCEP for SOFC anode material. The distributions of Ni and Zr in grain boundary caused by molecular diffusion were quantified at different sintering temperatures in the range 1,100 °C–1,300 °C. The effects of sintering on nanosurface and structural properties of CMCEP were analyzed through scanning electron and back-scattered electron microscopies and specific surface area. The crystallinity of CMCEP was found to increase with increasing sintering temperature. Smoothing, neck formation, shrinkage, and densification of nano-sized NiO-8YSZ composite granules occurred due to the acceleration of molecular diffusion at sintering temperatures above 1,200 °C, resulting in distinct grain boundary formation. The width of interfacial transition gap between Ni and Zr measured with respect to the grain boundary increased by 69.1% as molecular diffusion accelerated with increasing sintering temperature from 1,100 to 1,300 °C. The results of the nanostructural analysis of the CMCEP surface showed a decrease in the specific surface area (measured by the Brunauer Emmett Teller (BET) method) with increasing calcination temperature. The results of this study are expected to contribute to performance optimization in the future via the control of the porosity, electrical conductivity, and triple phase boundary generation during SOFC anode layer production using plasma sprays.

(Received July 21, 2017; Accepted October 19, 2017)

Keywords: Sintering, Nanostructure, Grain boundary, Diffusion, NiO, 8YSZ

1. Introduction

Solid oxide fuel cell (SOFC) is an electrochemical energy conversion device that converts fuel to electrical energy through chemical reactions. This research field has received attention owing to various advantages such as high efficiency, environmental friendliness, and low noise. Despite these advantages, the high production cost of SOFC, low durability, and difficulty in manufacturing and processing of raw materials have been mentioned as problems that need to be solved [1]. To overcome the shortcomings of SOFC, the metal-supported solid oxide fuel cell

*Corresponding author: jmjung@jbnu.ac.kr

†The two authors were equally contributed to this article.

(MSC) technology has been proposed to improve strength using metal-ceramic bonding. Unlike other SOFC types, MSC has advantages of outstanding cost-efficiency, high mechanical strength, and ease of processing since it uses a low-cost porous metal as a support [2-5].

Plasma spraying is one of the typical dry processes used to produce SOFC anodes. Metal-supported SOFC can be fabricated by effectively depositing an anode functional layer on metallic anode through the plasma spraying process [6-8]. Calcined micro-sized nickel oxide-8 mol% yttria-stabilized zirconia (NiO-8YSZ) cermet particle—using Ni and Zr as raw materials—can be utilized as stock powder for SOFC anode in the plasma spraying process. Ni has advantages of low cost and excellent catalytic properties for high fuel gas; YSZ maintains its porous structure even at high temperatures, promoting the triple phase boundary (TPB) [9-11]. In addition, the electrical conductivity between Ni and YSZ is outstanding.

Calcined micro-sized NiO-8YSZ cermet particle (CMCEP) can be prepared by spray drying granulated nanosize-milled Ni and 8YSZ and calcining through sintering process. In particular, as-sprayed micro-sized NiO-8YSZ composite particles (AMCOP), which are packed nano-sized NiO-8YSZ composite granules prepared by spray drying, went through a series of processes such as smoothing, neck formation, shrinkage, densification, and grain growth due to diffusion induced by high temperature during sintering. As a result, grain boundaries between NiO and 8YSZ were formed after sintering and the grains were consolidated, densified, and coarsened through physicochemical reactions, generating electrical conductivity, porosity, and TPB for anode function in CMCEP [12-14].

In the case of CMCEP formed by sintering under various conditions, the circulation of fuel gas becomes straightforward with increasing porosity. Moreover, the TPB generated within a particle acts as an electrochemical active point for the reaction of electrons, oxide ions, and gas at Ni, YSZ, and open pore convergences. Mobilities of activated electrons and ions in TPB are determined by electrical conductivity across Ni and Zr grain boundaries. Accordingly, SOFC performance is highly determined by the nanostructural and electrical properties of the anode such as electrical conductivity, porosity, and TPB [10, 11]. Most studies on microstructure and the physical and electrical properties of SOFC have been conducted intensively using planar SOFC, tubular SOFC, or functional layers prepared by a printing or coating method. For example, Nguyen et al. [15] studied the effect of sintering temperature and applied load on SOFC performance after preparing a flat SOFC cell using a 5:5 NiO/YSZ anode and 3:7 NiO/YSZ anode functional layer. Talebi et al. [16] evaluated the microstructures and electrochemical impedances of YSZ electrolyte films prepared from NiO, YSZ, and starch powders in the 5:5:2 ratio.

Nevertheless, the nanostructure of CMCEP used as stock powder during plasma spray to produce SOFC anode may be the key factor determining the performance of SOFC anode. The nanostructure and electrical properties can be determined through the proper adjustment of calcination conditions during CMCEP production. When CMCEP was prepared by calcining spray-dried AMCOP, the molecular diffusion and grain growth patterns varied with calcination condition. Nanostructural properties such as grain boundary, specific surface area, and porosity were different. As a result, changes in CMCEP nanostructure determine electrical conductivity, porosity, and TPB, which are important factors that determine SOFC anode performance.

The purpose of this study was to analyze the effect of the sintering temperature on the nanostructure and diffusion of calcined micro-sized Ni-8YSZ cermet particles used in the plasma spraying process to produce SOFC anode layers. During CMCEP production by sintering, grain boundary formation (due to diffusion) was observed and the molecular diffusion of Ni and Zr were analyzed quantitatively. In addition, the effect of sintering on nanosurface and structural properties of CMCEP was analyzed.

2. Experimental

2.1 Materials

NiO (Kceracell, South Korea) and 8YSZ (Kceracell, South Korea) were purchased to prepare the slurry used in the spray drying process. First, 200 g polycarboxylate ammonium salt (5468CF, SAN NOPCO, South Korea) was added into 40 L distilled water as dispersant, followed

by 30 wt% of NiO and 8YSZ in 3:2 wt% ratio. The mixture was continuously mixed at 600 rpm using a stirrer for homogenization. Next, 160 g polyvinyl alcohol (PVA)/polyether mixture (HS-BD-25, SAN NOPCO, South Korea) was added as binder. The NiO-8YSZ composite slurry was prepared by milling for 22 h [17].

2.2 Spray drying

The NiO-8YSZ composite slurry prepared by mixing and milling was supplied to a spray drier (FS-1.5D, Fine Tech, South Korea) at a flow rate of 250 mL/h. The atomizer disk of the spray drier was rotated at 12,000 rpm and the prepared slurry was sprayed to make droplets. The droplets contacted hot gas at 180 °C inside the spray drier [17]. The nano-sized NiO-8YSZ composite was packed and granulated, resulting in spherical AMCOP.

2.3 Sintering

CMCEP was prepared by sintering using the AMCOP. The AMCOP collected in the spray drier was subjected to heating and cooling during sintering in a furnace. Neck formation, densification, and grain growth of NiO-8YSZ occurred during the sintering process [18]. The calcination process started from the debinding stage and the internal temperature of the furnace (where the AMCOP was located) was increased to 325 °C at 1.5 °C/min. After maintaining temperature at 325 °C for 150 min, the internal furnace was increased at 4.0 °C/min to 1,100, 1,150, 1,200, 1,250, or 1,300 °C depending on sample preparation condition. After calcination for 150 min, the CMCEP sample was cooled down slowly to room temperature using the furnace cooling process.

2.4 Nanostructural characterization

Phase compositions of NiO and 8YSZ were determined using a multi-purpose high performance X-ray diffractometer (XRD) (X'pert Pro Powder, PANalytical, Netherlands). Morphology and nanostructure of CMCEP were observed using a field-emission scanning electron microscope (FE-SEM; SU-70, HITACHI, Japan) at 10,000× magnification. Additionally, the grain boundary formation of the CMCEP nanostructure was analyzed using the back-scattered electron microscopy (BSE) mode of FE-SEM (SUPRA 40VP, Carl Zeiss, Germany) at 35,000× magnification. In principle, BSE exhibits different contrasts depending on atomic number. For the analysis, all CMCEPs were rigidly mounted using carbon conductive adhesive tapes.

Energy dispersive spectroscopy (EDS; SU-70, HITACHI, Japan) analysis was performed to observe grain boundary formation of the packed nano-sized NiO-8YSZ composite granules within AMCOP prepared by spray drying due to elemental diffusion during sintering. Diffusion of Ni and Zr was quantitatively analyzed according to sintering temperature by performing 2D line profile analysis on the Ni-Zr grain boundary.

To measure the specific surface area of CMCEP, a surface area analyzer (BELSORP-max, BEL, Japan) applying the Brunauer Emmett Teller (BET) method was used. Before loading the sample into the device, pretreatment at 250 °C was carried out for 12 h to remove moisture or gas adsorbed on particle pores. Measurements were made at various points to obtain correlation coefficient larger than 0.999 while changing the pressure under isothermal conditions using N_2 gas.

3. Results and discussion

Fig. 1 shows XRD patterns of calcined CMCEP prepared at different sintering temperatures. Control refers to the XRD pattern of AMCOP before sintering. Overall, only NiO and YSZ phases were observed in all patterns before and after sintering. The intensity of the YSZ phase increased with increasing sintering temperature, indicating an increase in YSZ crystallinity with calcination.

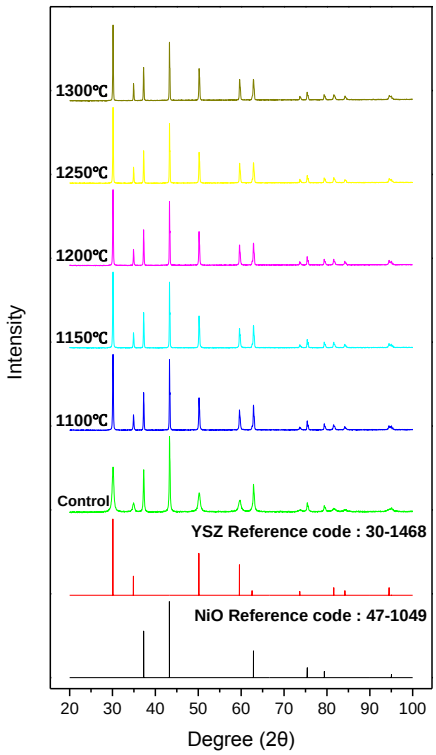

Fig. 1. XRD patterns of calcined micro-sized NiO-8YSZ cermet particle (CMCEP) at different sintering temperatures. Control indicates as-sprayed micro-sized NiO-8YSZ composite particle (AMCOP).

Fig. 2 shows SEM images of CMCEP nanostructures generated from the spray-dried spherical AMCOP (control) by sintering in the temperature range 1,100–1,300 °C. Nano-sized NiO-8YSZ composite granules of the spherical AMCOP generated after spray drying were packed heterogeneously in Fig. 2(a). As shown in Fig. 2(b), the grain boundary was not sufficiently formed due to insufficient molecular diffusion during sintering at 1,100 °C. At 1,150 °C (Fig. 2(c)), a mixture of calcined NiO-8YSZ grains and non-calcined nano-sized NiO-8YSZ composite granules was observed after the formation of grain boundaries induced by diffusion. In Fig. 2(d), the grain boundary between Ni and Zr was clearly formed at temperature above 1,200 °C. When sintering temperature was gradually increased to 1,250 °C and 1,300 °C, diffusion was promoted and the grain size gradually increased due to NiO-8YSZ grain growth.

Processes such as smoothing, neck formation, shrinkage, densification, and grain growth of heterogeneously packed nano-sized NiO-8YSZ composite granules caused by molecular diffusion during sintering were successfully analyzed from Fig. 2(b–f). Since the molecular diffusion that causes neck formation, densification, and grain growth became more active with the increase in energy due to increasing calcination temperature, the grain boundary became more distinct and grain growth was promoted.

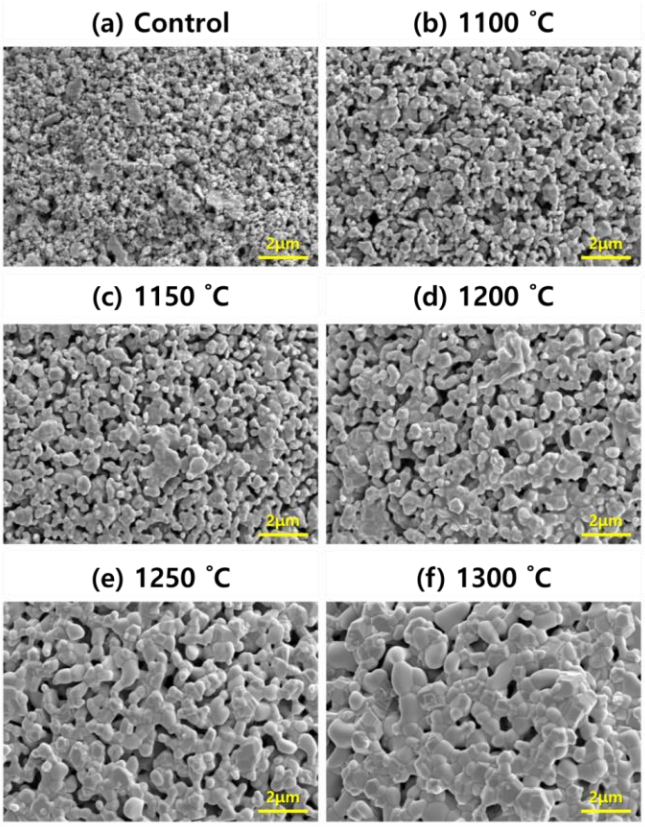

Fig. 2. SEM surface image of calcined micro-sized NiO-8YSZ cermet particle (CMCEP) prepared by sintering (10,000× magnification). Control indicates as-sprayed micro-sized NiO-8YSZ composite particle (AMCOP).

Fig. 3 shows 35,000× magnification SEM and BSE images of nano-sized NiO-8YSZ grains within CMCEP at different sintering temperatures. As can be seen in the first column of Fig. 3, the early stage of smoothing could be observed from nano-sized NiO-8YSZ composite granules of spherical AMCOP generated by spray drying at 1,100 °C. However, nano-sized NiO-8YSZ composite granules could not be bonded and existed heterogeneously due to insufficient diffusion. The grain boundary began to form at 1,150 °C, but formation was still insufficient. After smoothing, necking between nano-sized NiO and 8YSZ granules in most nano-sized NiO-8YSZ composite granules started at 1,200 °C and the nanostructure gradually became denser with increasing sintering temperature, resulting in distinct grain boundary formation. When the sintering temperature was gradually increased to 1,250 °C and 1,300 °C, molecular diffusion was promoted and the size of NiO-8YSZ grains increased gradually.

BSE images are shown in the second column of Fig. 3 to examine diffusion between NiO-8YSZ more accurately. The bright (see yellow arrow) and dark (see green arrow) parts of the BSE image in Fig. 3 represent Zr and Ni, respectively. Almost no diffusion of nano-sized NiO-8YSZ composite granules was observed in the BSE image of the 1,100 °C sample. Grains were not formed and distribution was not homogeneous. This result is consistent with the findings from SEM images. Neck formation began to occur in which dark Ni and bright Zr between nano-sized NiO-8YSZ composite granules started to connect by diffusion at 1,150 °C. However, the grain boundary between NiO and 8YSZ was still not clearly formed. As the calcination temperature increased above 1,200 °C, grain boundaries between NiO and 8YSZ particles formed clearly due to the more active diffusion. When the calcination temperature reached 1,250 °C and 1,300 °C, grain growth was further accelerated and the grain boundary could be distinguished more clearly.

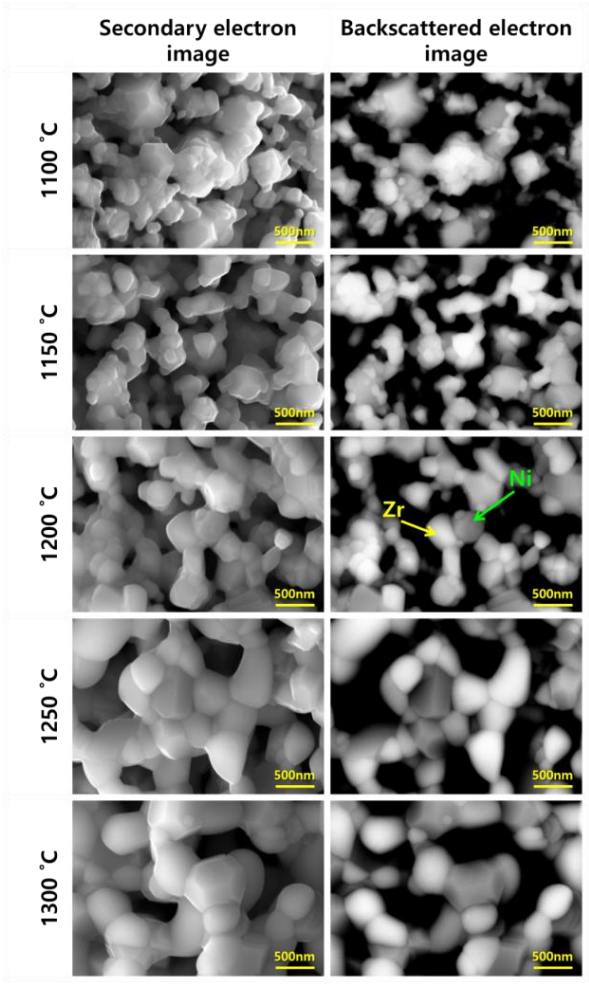

Fig. 3. Scanning electron microscopy (SEM) and back-scattered electron microscopy (BSE) images of NiO-8YSZ grains within calcined micro-sized NiO-8YSZ cermet particle (CMCEP) prepared by sintering (35,000× magnification). In the BSE images, yellow and green arrows indicate Zr and Ni, respectively.

To quantitatively analyze the effect of the sintering temperature on the grain boundary formation and molecular diffusion of CMCEP, the EDS line profile scan technique was used, as shown in Fig. 4(a). The diffusion of Ni and Zr could be quantified through the analysis of the interfacial transition region size at the grain boundary. The x-axis of the graph shown in Figs. 4(b–f) represents the length of the EDS line profile, which is a straight line across the grain boundary, while the y-axis represents the region of interest (ROI) value, which is the relative concentration of the corresponding molecule [19]. The horizontal black solid line and the red dotted line in the left region of the graph indicate the maximum concentration of Ni and the minimum concentration of Zr, respectively, indicating the absence of Zr diffusion. Meanwhile, the horizontal black solid line and the red dotted line in the right region of the graph indicate the maximum concentration of Zr and the minimum concentration of Ni, respectively, indicating the absence of Ni diffusion. Thus, the width of the interfacial transition region between the horizontal black solid line and the red dotted regions could quantify the extent of interfacial molecular diffusion.

As can be seen from Fig. 4(b–f), the width of the interfacial transition region increased with calcination temperature. The size of the interfacial transition region of CMCEP calcined at 1,100 °C (Fig. 4(b)) was 340 ± 24.43 nm, while the width of the interfacial transition region gradually increased with increasing calcination temperature. In Fig. 4(f), the width of the interfacial transition region reached its maximum value of 575 ± 21.21 nm at calcination

temperature of 1,300 °C. Compared to that at 1,100 °C, molecular diffusion of more than 69.1% was induced. The increase in width of the interfacial transition region by molecular diffusion might be related to the improvement of the electrical conductivity affecting the migration of electrons and oxide ions generated in the TPB, the electrochemically active site of the SOFC anode [20].

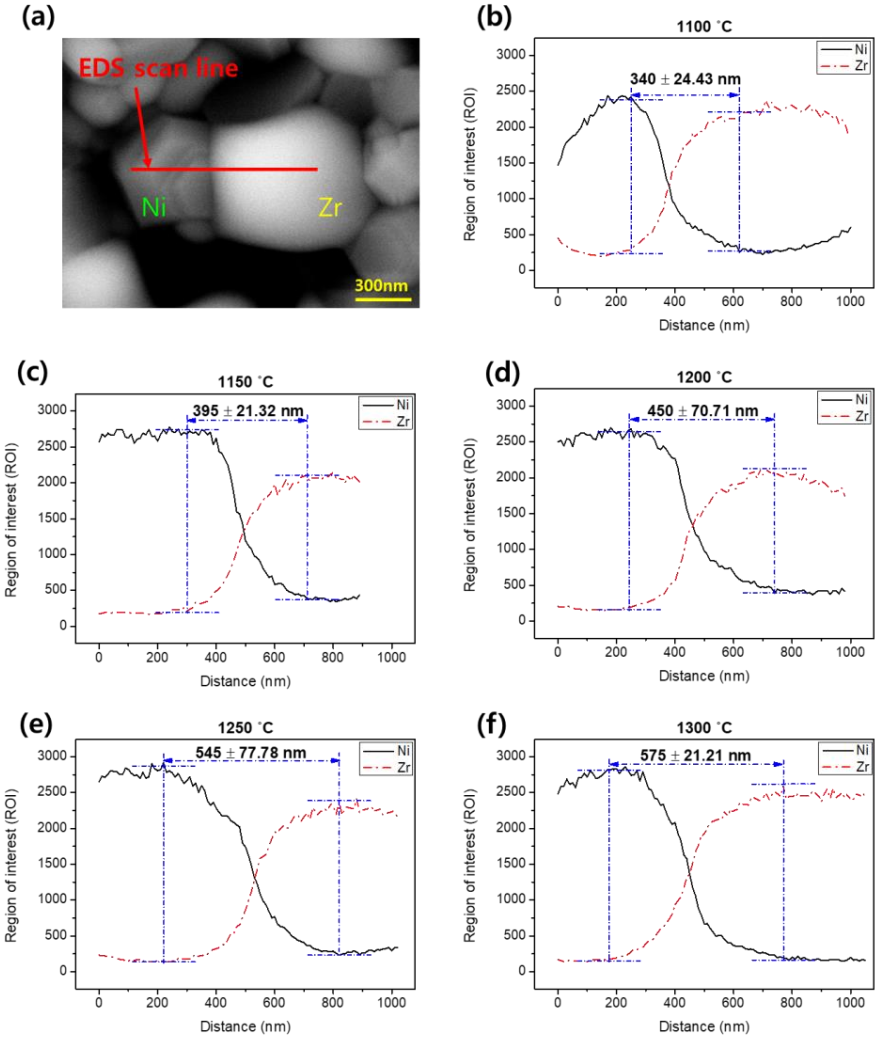

Fig. 4. Diffusive distribution of Ni and Zr molecules across grain boundaries at different sintering temperatures.

The specific surface area of particles is known to be closely related to porosity and TPB formation, contributing to the overall SOFC performance [8, 12]. Thus, the specific surface area of CMCEP prepared at different sintering temperatures was analyzed in this study and the results are shown in Fig. 5. BET value of AMCOP before calcination was 10.79 m^2/g, while BET value of CMCEP formed after calcination was significantly lower. The significant difference in BET value before and after calcination was due to smoothing and densification caused by the diffusion of packed nano-sized NiO-8YSZ composite granules during CMCEP formation through the calcination process. Interestingly, as the calcination temperature was increased continuously to 1,100, 1,150, 1,200, 1,250 and 1,300 °C, the BET values of CMCEP tended to decrease gradually to 2.20, 1.61, 1.34, 0.59 and 0.46 m^2/g, respectively. Molecular diffusion became more active as the calcination temperature was increased up 1,300 °C, accelerating NiO-8YSZ grain growth and resulting in the reduced specific surface area.

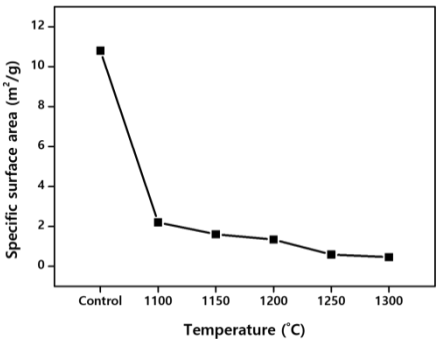

Fig. 5. Specific surface area measured by the Brunauer Emmett Teller (BET) method at different sintering temperatures. Control indicates as-sprayed micro-sized NiO-8YSZ composite particle (AMCOP).

Electrical conductivity, porosity, and TPB, which are the three major physical properties related to the performance of an SOFC anode did not show proportional correlations with each other. The increased electrical conductivity due to improving grain growth could lead to a relative decrease in BET, causing a decrease in porosity. In the case of the SOFC anode, the increased porosity due to increased specific surface area might improve performance by promoting redox reactions on the surface, but it could lead to a relative reduction in electrical conductivity.

4. Conclusions

In this study, the effects of the sintering temperature on the nanostructure and diffusion of CMCEP during NiO-8YSZ synthesis (for SOFC electrode material) were analyzed. Increase in CMCEP crystallinity was confirmed with increasing sintering temperature. From SEM images, the grain boundary formation of nano-sized NiO-8YSZ composite granules in CMCEP via smoothing, neck formation, shrinkage, and densification processes by molecular diffusion was successfully examined as a function of sintering temperature. In particular, BSE images confirmed the distinct grain boundaries between Ni and Zr at calcination temperatures above 1,200 °C and the grain growth with increasing temperature.

The characteristics of molecular diffusion between Ni and Zr were quantified by measuring the size of the interfacial transition region at the grain boundary. The width of the interfacial transition region increased in proportion to the elevation of sintering temperature and the molecular diffusion became more active by about 69.1% when the sintering temperature was increased from 1,100 to 1,300 °C. From the results of the nanostructural analysis of the CMCEP surface, the specific surface area tended to decrease continuously with increasing calcination temperature. In this study, the nanostructure and diffusion characteristics of CMCEP were successfully analyzed based on sintering temperature. The corresponding results are expected to contribute to future performance optimization during MSC anode production using plasma spray.

Acknowledgements

The authors would like to acknowledge Mr. Choong Hwan Lee for his assistance in preparing samples for analysis. This work was also supported by the National Research Foundation of Korea (grant no. NRF-2016R1C1B2014747 and NRF-2016R1D1A3B03935132).

References

[1] M.C. Tucker, J Power Sources, **195**, 4570 (2010).
[2] J. Mougin, A. Brevet, J.C. Grenier, R. Laucournet, P.O. Larsson, D. Montinaro, L.M. Rodriguez-Martinez, M.A. Alvarez, M. Stange, S. Trombert, ECS Trans, **57**, 481 (2013).
[3] J. Laurencin, V. Roche, C. Jaboutian, I. Kieffer, J. Mougin, M.C. Steil, Int J Hydrogen Energ, **37**, 12557 (2012).
[4] P. Blennow, J. Hjelm, T. Klemensø, S. Ramousse, A. Kromp, A. Leonide, A. Weber, J Power Sources, **196**, 7117 (2011).
[5] S.W. Baek, J. Jeong, H. Schlegl, A.K. Azad, D.S. Park, U.B. Baek, J.H. Kim, Ceram Int, **42**, 2402 (2016).
[6] R. Henne, J Therm Spray Techn, **16**, 381 (2007).
[7] R. Hui, Z. Wang, O. Kesler, L. Rose, J. Jankovic, S. Yick, R. Maric, D. Ghosh, J Power Sources, **170**, 308 (2007).
[8] B. Shri Prakash, S. Senthil Kumar, S.T. Aruna, Renew Sustainable Energy Rev, **36**, 149 (2014).
[9] D. Simwonis, A. Naoumidis, F. Dias, J. Linke, A. Moropoulou, J Mater Res, **12**, 1508 (1997).
[10] S. Primdahl, M. Mogensen, J Electrochem Soc, **146**, 2827 (1999).
[11] J.W. Moon, G.D. Kim, K.T. Lee, H.L. Lee, J Korean Ceram Soc, **38**, 466 (2001).
[12] D. Stöver, H.P. Buchkremer, S. Uhlenbruck, Ceram Int, **30**, 1107 (2004).
[13] R. Saptono, Procedia Eng, **50**, 369 (2012).
[14] H. Djohari, J.J. Derby, Chem Eng Sci, **64**, 3810 (2009).
[15] X.V. Nguyen, C.T. Chang, G.B. Jung, S.H. Chan, W. Huang, K.J. Hsiao, W.T. Lee, S.W. Chang, I.C. Kao, Energies, **9**, 701 (2016).
[16] T. Talebi, M. Haji, B. Raissi, Int J Hydrogen Energ, **35**, 9420 (2010).
[17] I. Hwang, J. Jeong, K. Lim, J. Jung, Ceram Int, **43**, 7728 (2017).
[18] M. Steil, F. Thevenot, M. Kleitz, J Electrochem Soc, **144**, 390 (1997).
[19] L.V. Saraf, Electrochem Solid St, **14**, B100 (2011).
[20] Q. Yang, B. Meng, Z. Lin, X. Zhu, F. Yang, S. Wu, Ionics, **23**, 967 (2017).